Journal of Environmental Management 371 (2024) 123269

Contents lists available at ScienceDirect

Journal of Environmental Management

journal homepage: www.elsevier.com/locate/jenvman

Research article

Direct Ag-Hg amalgamation in the nanoscale on the surface of biosourced amorphous silica

V.J. Inglezakis [a,*], S. Azat [b,c], N. Kinayat [d], A. Guney [e], Z. Baimenova [b], Z. Tauanov [c,f,**]

[a] Department of Chemical and Process Engineering, University of Strathclyde, Glasgow, UK
[b] Laboratory of Engineering Profile, Satbayev University, Satbayev St., Almaty, Kazakhstan
[c] LLP Scientific Production Technical Center "Zhalyn", Almaty, Kazakhstan
[d] Department of Chemical & Materials Engineering, School of Engineering & Digital Sciences, Nazarbayev University, Astana, Kazakhstan
[e] Department of Civil and Environmental Engineering, School of Engineering & Digital Sciences, Nazarbayev University, Astana, Kazakhstan
[f] Ecology Research Institute, Khoja Akhmet Yassawi International Kazakh-Turkish University, Turkestan, Kazakhstan

ARTICLE INFO

Keywords:
Rice husk silica
Silver nanoparticles
Nanocomposites
Triethoxicilane
Mercury
Calomel
Amalgamation

ABSTRACT

Mercury poses a significant threat to air, soil, and water ecosystems. Mercury-based alloys, aka amalgams, are already known for their effectiveness in mercury capture in water and gaseous streams. However, limited research has been published on direct amalgamation, the process involving a direct redox reaction between two metals, occurring on the surface of amorphous silica. This study investigates the amalgamation process in nanoscale, in particular the direct interaction between silver (Ag^0) nanoparticles supported on functionalized bio-derived amorphous silicon dioxide (SiO_2) and mercury (Hg^{2+}) ions in aqueous solutions. Also, the influence of aqueous mercury speciation on amalgamation is studied in detail. The results reveal that the presence of chloride (Cl^-), acetate (OAc^-), and nitrate (NO_3^-) ions significantly influences the interaction between mercury and silver. We propose plausible mechanisms to explain these observations. Our findings demonstrate that the maximum mercury uptake capacity followed the order $HgCl_2 > Hg(OAc)_2 > Hg(NO_3)_2$, while the reaction rate followed the order $Hg(OAc)_2 > HgCl_2 > Hg(NO_3)_2$. These findings hold significant implications for the design of efficient mercury remediation processes. By elucidating the influence of aqueous speciation on amalgamation, our work paves the way for tailored strategies that can maximize mercury capture from water.

1. Introduction

Bimetallic nanoparticles have gained significant interest due to their tunable characteristics, making them promising candidates in various fields related to environmental applications, including catalysis, sensors, and water treatment (Harika et al., 2020; Kim et al., 2023). Notably, nanoalloys exhibit distinct properties compared to their individual components, offering advantages like enhanced electrocatalytic activity (Liu and Huang, 2013; Mertens et al., 2011). This paper is on amalgamation, a process where mercury binds with other metals, as a strategy for mercury capture from contaminated water. While elemental mercury is highly toxic, its amalgamation with specific metals renders it significantly less harmful (Harika et al., 2020).

Amalgamation in the aqueous phase requires the reduction of Hg^{2+} to Hg^0 and this can happen chemically by a reducing agent added in the solution, electrochemically by an anode-cathode system or by a direct redox reaction involving the oxidation of another metal with lower reduction potential (Table 1). For instance, Tunsu and Wickman (2018) employed electrochemical reduction for the removal of Hg^{2+} from aqueous solutions on Pt^0 thin films (100 nm) by the formation of Pt-Hg alloy at the Pt cathode. An example of a chemically assisted amalgamation is this of Au-Hg amalgamation where several reducing agents have been used to reduce Hg^{2+} so to react with Au^0 such as $NaBH_4$ (Schopf et al., 2015, 2017), sodium citrate ions (Ojea-Jiménez et al., 2012) and ascorbic acid (Xu et al., 2018). There are some studies on direct Au-Hg amalgamation, as this of Mertens et al. (2011) and Ag-Hg amalgamation, e.g. Katok et al. (2012). Finally, ultrasonic-assisted amalgamation has been reported or the formation of Pd-Hg amalgams from a mixture of liquid Hg^0 and Pd^{2+} (Harika et al., 2020) and Ag-Hg amalgams from a mixture of Hg^0 and Ag^+ in aqueous solutions (Harika et al., 2018). While

* Corresponding author.
** Corresponding author. LLP Scientific Production Technical Center "*Zhalyn*", Almaty, Kazakhstan.
E-mail addresses: vasileios.inglezakis@strath.ac.uk (V.J. Inglezakis), zhtauanov@nu.edu.kz (Z. Tauanov).

https://doi.org/10.1016/j.jenvman.2024.123269
Received 12 August 2024; Received in revised form 1 November 2024; Accepted 4 November 2024
Available online 8 November 2024

Table 1
Standard reduction potentials (SHE) (Bratsch, 1989; Harris, 2007; Karp, 2008; Kobayashi et al., 2016).

Half reaction	Reduction potential (V)
$H_2 + 2e^- \rightleftharpoons 2H^-$	−2.40
$C_2H_3O_2^- + 2H^+ + 2e^- \rightleftharpoons C_2H_4O$	−0.58
$Hg_2Cl_2 + 2e^- \rightleftharpoons 2Hg^0 + 2Cl^-$	+0.27
$Hg_2^{2+} + 2e^- \rightleftharpoons 2Hg^0$	+0.80
$Ag^+ + e^- \rightleftharpoons Ag^0$	+0.80
$Hg^{2+} + 2\,e^- \rightleftharpoons Hg^0$	+0.85
$2NO_3^- + 10H^+ + 8e^- \rightleftharpoons NH_4^+ + 3H_2O$	+0.88
$Pd^{2+} + 2e^- \rightleftharpoons Pd^0$	+0.92
$2\,Hg^{2+} + 2\,e^- \rightleftharpoons Hg_2^{2+}$	+0.91
$Pt^{2+} + 2e^- \rightleftharpoons Pt^0$	+1.18
$2NO_3^- + 12H^+ + 10e^- \rightleftharpoons N_2(g) + 6H_2O$	+1.25
$Cl_2(g) + 2e^- \rightleftharpoons 2Cl^-$	+1.36
$Au^{+3} + 3e^- \rightleftharpoons Au^0$	+1.50

avoiding the use of chemicals electrochemical and direct reduction come with trade-offs: the former are complex and expensive, while the latter might contaminate the solution with oxidized ions.

Substantial research has been conducted on direct amalgamation, but knowledge gaps remain, especially regarding the behaviour on solid surfaces, which warrants further exploration (Table 2). As the reduction potential of mercury is higher than this of silver, in the presence of Hg^{2+} the following redox reaction takes place (Table 1):

$$Hg^{2+} + 2Ag^0 \rightarrow Hg^0 + 2Ag^+ \quad (1)$$

Then, Hg^0 and Ag^0 form Ag-Hg amalgams (Katok et al., 2012). The relevant studies showed that Hg_2^{2+}, Ag^0 and Ag-Hg amalgams are stable on the surface of SiO_2 (Katok et al., 2012, 2013). In a paper published in 1982 Pang and Richie (Pang and Ritchie, 1982) studied the reactions between mercury ions in aqueous solution containing HNO_3 and silver discs of 3 cm diameter. Electrochemical kinetics were measured galvanostatically and simple kinetics by immersing a silver disc in mercury solutions. The authors identified the following reactions:

$$Hg^{2+} + Ag^0 \rightarrow 0.5Hg_2^{2+} + Ag^+ \quad (2)$$

$$0.5Hg_2^{2+} + Ag^0 \rightarrow Hg^0 + Ag^+ \quad (3)$$

$$Hg^{2+} + 2Ag^0 \rightarrow Hg^0 + 2Ag^+ \quad (4)$$

Reaction (2) is called dissolution reaction and reactions (3) and (4) displacement reactions. The authors found that at temperatures below 35 °C the dissolution reaction predominates and above 35 °C the displacement reaction (4) predominates. Other studies have shown that this temperature could be 28 °C and that near this temperature both reactions occur (Pang and Ritchie, 1982). Based on the reduction potentials (Table 1), the dissolution reaction and the displacement reaction (4) are favored, but not the displacement reaction reaction (3). Thus, the reduction of Hg^{2+} to Hg_2^{2+} and Hg^0 most probably happen in parallel rather than stepwise. Despite extensive research using electrochemical cells to investigate Hg^{2+} reduction, the mechanism remains debated. The key question is whether the reduction proceeds in a single step to Hg^o or involves an intermediate Hg_2^{2+} species. Studies show pH and speciation in solution impact how the reaction proceeds (Serruya et al., 1999). For instance, the formation of Hg complexes in the aqueous phase alters the reduction potential of Hg^{2+} and the formation of $HgOH^-$ in neutral solution should result in slightly less positive reduction potential than +0.85V (Henglein and Brancewicz, 1997). To the best of our knowledge, the simultaneous reduction of Hg^{2+} to both Hg_2^{2+} and Hg^o in aqueous solutions using supported Ag^o nanoparticles is documented only by Inglezakis et al. (2021).

Besides the redox path, the products of the Ag-Hg amalgamation vary, even in simple solutions. For instance, Harika et al. (2018) studied the interaction of Hg^0 (liquid form) and Ag^+ in aqueous solution under sonication. The reduction potentials show that the Ag^+ reduction cannot happen (Table 1) however ultrasonic cavitation in aqueous solution allows this reduction to take place. The results showed that the reaction products depend on the Ag:Hg molar ratio and for 0.33–1 a non-crystalline Ag-Hg mixture was formed, for 0.5–0.67:1 moschellandbergite (Ag_2Hg_3), for 1.5:1 schacherite ($Ag_{1.1}Hg_{0.9}$), and for 1:1 a mixture both, whereas for the range of 2–6:1 no amalgam was formed. When completing agents, such as Cl^-, present in the solution, more reactions and products are possible. Wang et al. (2019) used $HgCl_2$ to investigate the removal of Hg^{2+} from water by Ag^0@covalent organic frameworks nanocomposite and XRDs showed the formation of AgCl and $Ag_{1.1}Hg_{0.9}$. Sumesh et al. (2011) used $HgCl_2$ to study the removal of Hg^{2+} from water by use of Ag^0@alumina nanocomposite and XRD identified a different amalgam, namely Ag_3Hg_2. Tauanov et al. worked on mercury removal from $HgCl_2$ solutions and identified calomel on the surface of Ag^0@synthetic zeolites (analcime and sodalite) (Tauanov et al., 2020). Focusing on Ag^0@silica, Yordanova et al. (2014) studied the influence of NO_3^- and Cl^- on Hg-Ag amalgamation in water phase by use of Ag^0@silica nanocomposite and found that Ag_2Hg_3 is formed, however, the nanocomposite used besides Ag^0 was decorated with NH_2 groups which contributed to the removal of Hg^{2+}. Katok et al. (2012) used $Hg(NO_3)_2$ and $Hg(OAc)_2$ solutions but only the results of $Hg(NO_3)_2$ were presented. Azat et al. studied the removal Hg^{2+} from $HgCl_2$ solution and identified several potential compounds including calomel and Hg-Ag amalgams but the XRDs were inconclusive (Azat et al., 2020). Inglezakis et al. (2021) studied the same system and observed the coexistence of calomel and two amalgams, Ag_2Hg_3 and $Ag_{1.1}Hg_{0.9}$, for first time in the literature. Concerning other amalgams, Tunsu and Wickman (2018) studied the Pt-Hg amalgamation and found that the presence of Cl^- ions does not affect the uptake of Hg^{2+} from the aqueous phase. Both $Hg(NO_3)_2$ and $HgCl_2$ were used in a study on Au-Hg amalgamation with no significant effects on the removal efficiency (Ojea-Jiménez et al., 2012). Lisha et al. studied the Hg-Au amalgamation in $HgCl_2$ solution and found no other compounds besides the amalgam (Lisha et al., 2009). On the other hand, Wang et al. (2016) who studied the electrochemical formation of Hg-Au amalgam used a specific method to avoid calomel formation. In a study on photocatalytic reduction of Hg^{2+} over Au@TiO_2, the presence of chlorides resulted in the formation of Hg_2Cl_2 while in the absence of chlorides the removal of mercury proceeds through the formation of Hg–Au amalgams (Spanu et al., 2019). Pasakarnis et al. (2013) studied the effects of chloride and Fe^{2+} content on the reduction of Hg^{2+} by magnetite. The results showed that in the absence of chloride, reduction of Hg^{2+} to Hg^0 is observed while in the presence of chloride metastable Hg_2^{2+} calomel species were formed for the more oxidized magnetite particles.

The literature review demonstrates that, especially for Ag-Hg amalgamation, the formation of other compounds, such as calomel (Hg_2Cl_2), has been rarely observed and not thoroughly studied. Besides the redox path and the reaction products there are few studies on the Ag-Hg amalgamation in nanoscale in aqueous solutions (Table 2). In these studies, the identification of the formed amalgams is not always done, the discussion on the amalgamation mechanism is rather limited and the effect of anions and thus, speciation of Hg^{2+} in the aqueous phase on Hg-Ag amalgamation is not systematically studied. The objective of this work was to investigate the effectiveness of a sustainable adsorbent towards mercury and investigate the mechanisms involved and the role of aqueous phase speciation of Hg. This is of particular importance as the mercury speciation in water can affect the surface interactions, alter the sorption mechanism, and thus enhance or hinder its removal. This is a continuation of our previously published work (Inglezakis et al., 2021) extending the study to $Hg(NO_3)_2$ and $Hg(OAc)_2$ solutions and a more detailed discussion on mechanisms.

Table 2
Literature review on aqueous phase Hg-Ag amalgamation in nanoscale.

Solid phase	Liquid phase	Interaction	Formed compounds	Reference
Supported NPs				
Ag^0 NPs@silica	$Hg(NO_3)_2$ $HgCl_2$ $Hg(OAc)_2$ $C_o = 200$ ppm $pH_o = 2–4.5$	Direct	$Ag_{1.1}Hg_{0.9}$ Hg_2Cl_2 AgCl	This work
Ag^0 NPs@silica	$HgCl_2$ $C_o = 300$ ppm $pH_o = 3.5$	Direct	$Ag_{1.1}Hg_{0.9}$ Ag_2Hg_3 Hg_2Cl_2 AgCl	Inglezakis et al. (2021)
Ag^0 NPs@silica[a]	$HgCl_2$ $C_o = 100$ ppm $pH_o = n/a$	Direct	Ag_2Hg_3 Ag_3Hg Hg_2Cl_2 HgO AgCl AgO	Azat et al. (2020)
Ag^0 NPs @synthetic zeolites[a]	$HgCl_2$ $C_o = 10$ ppm $pH_o = 2.5$	Direct	Hg-Ag amalgam	(Tauanov et al., 2018, 2019)
Ag^0 NPs @synthetic zeolites	$HgCl_2$ $C_o = 10–550$ ppm $pH_o = 2$	Direct	Hg_2Cl_2	Tauanov et al. (2020)
Ag^0 NPs @silica[b]	$Hg(NO_3)_2$ $Hg(OAc)_2$ $C_o = 0.15–312$ ppm $pH_o = 4–7$	Direct	$Ag_{1.1}Hg_{0.9}$	Katok et al. (2012)
Ag^0 NPs @covalent organic frameworks	$HgCl_2$ $C_o = 10$ ppm $pH_o = 5$	Direct	$Ag_{1.1}Hg_{0.9}$ AgCl	Wang et al. (2019)
Ag^0 NPs @silica	$HgCl_2$ $C_o = 50–200$ ppm $pH_o = 3.5–7$	Direct	Not specified	Ganzagh et al. (2016)
Ag^0 NPs @silica	$HgCl_2$ $C_o = 1–25$ ppb	Direct	Not specified	Azmi et al. (2023)
Ag^0 NPs @NH_2-silica	Hg^{2+} with HNO_3/HCl $C_o < 10$ ppb $pH_o = 2–7$	Surface decorated with NH_2 groups	Ag_2Hg_3 Hg^0	(Yordanova et al., 2014, 2022)
Ag^0 NPs@activated alumina	Hg^{2+} with HCl $C_o = 2$ ppm $pH_o = 2–12$	NPs protected by mercaptosuccinic acid	Ag_3Hg_2	Sumesh et al. (2011)
Ag^0 NPs@graphene oxide	Hg^{b+} $C_o = 2–40$ ppm	Direct	Hg-Ag amalgam[a]	Zangeneh Kamali et al. (2016)
Free NPs				
Ag^0 NPs solution	Hg^0 (liquid form)	Direct	$Ag_{1.1}Hg_{0.9}$	Liu and Huang (2013)
Ag^0 NPs solution	$Hg(NO_3)_2$	NPs protected by DNA	Hg-Ag amalgam[a]	Deng et al. (2013)
Ag^0 NPs @nylon membrane filters	Hg^{2+}	Direct	Hg-Ag amalgam[a]	Panichev et al. (2014)
Ag^0 NPs solution	$Hg(NO_3)_2$	Direct	Hg-Ag amalgam[a]	Fan et al. (2009)
Ag^0 NPs solution	Hg^{2+}	NPs coated with denatured bovine serum albumin	Not specified	Guo and Irudayaraj (2011)
Ag^0 NPs solution	Hg^{2+}	Direct	Hg-Ag amalgam[a]	Jarujamrus et al. (2015)
Ag^0 NPs gelatin stabilized	$HgCl_2$	Direct	Hg-Ag amalgam[a]	Jeevika and Shankaran (2016)
Ag^0 NPs colloid solution	$Hg(ClO_4)_2$	Exposed to γ-radiation	Hg-Ag amalgam[a] Hg^0 colloid	Katsikas et al. (1996)
Ag^0 NPs colloid solution	$Hg(ClO_4)_2$	Direct	Hg-Ag amalgam[a]	Henglein (1998)
Hg^0 liquid form	$AgNO_3$	Ultrasonic-assisted	$Ag_{1.1}Hg_{0.9}$ Ag_2Hg_3	Harika et al. (2018)
–	$Ag(ClO_4)$ $Hg(ClO_4)_2$	Sodium borohydride-assisted	$Ag_{1.1}Hg_{0.9}$	Henglein and Brancewicz (1997)
–	$Ag(ClO_4)$ $Hg(ClO_4)_2$	Sodium borohydride-assisted	$Ag_{1.1}Hg_{0.9}$	Yang et al. (2019)

[a] Inconclusive or absence of XRDs.
[b] The results of $Hg(OAc)_2$ are not presented in detail.

2. Materials and methods

2.1. Materials and chemicals

Triethoxysilane (TES, 95%), acetic acid (glacial, CH_3COOH), silver nitrate ($AgNO_3$, 99%), mercury chloride ($HgCl_2$, 98%) and sodium thiosulfate were purchased from Sigma Aldrich and used as received. The iodine (I_2, 0.05N) and sodium thiosulfate standard solutions (NaS_2O_3, 0.1N) were purchased from BioHimPribor (Kazakhstan) and used with appropriate dilution factor. All solutions were prepared using ultrapure water (UP) with a resistivity of 18.3 MΩ cm. The samples of rice husk (RH) obtained from the South Kazakhstan region was used as a raw material to produce synthetic silica. RH is an agricultural waste that is abundant in agro-based countries such as Kazakhstan and a sustainable source of silica. Our previous research has shown that high purity silica can be produced from RH using eco-friendly methods (Azat et al., 2019).

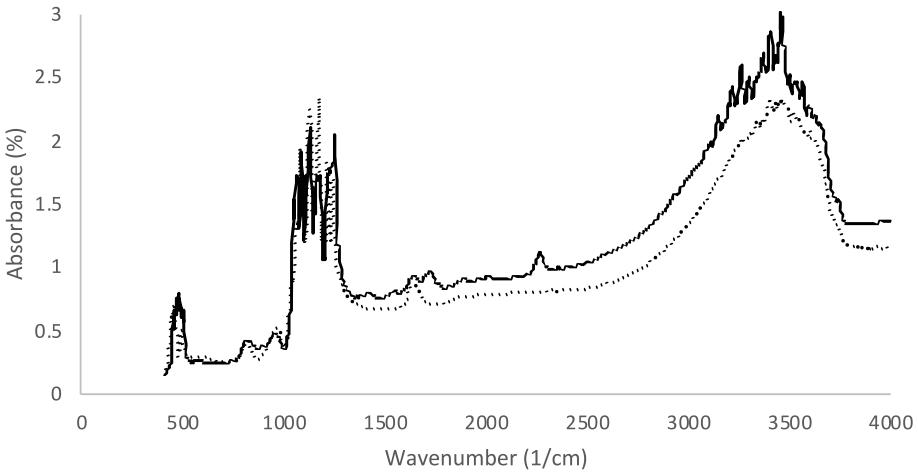

Fig. 1. FTIR spectra of SiO_2 (dotted) and TES-SiO_2 (solid) samples.

2.2. Synthesis of nanocomposites

The synthesis procedures for the biosourced SiO_2 from RH, the TES functionalization (TES-SiO_2) and the decoration with Ag^0 nanoparticles (Ag^0@SiO_2) are presented in our previous works (Azat et al., 2019; Inglezakis et al., 2021). Fresh materials were synthesized for this work and were fully characterized.

2.3. Mercury removal experiments

The adsorption performance of parent SiO_2, modified TES-SiO_2 and AgNPs@SiO_2 nanocomposites was tested using $HgCl_2$ solutions of 200 mg/L concentration without pH adjustment under ambient temperature and static conditions. In all experiments 0.1 g of samples were added into a conical flask containing 50 ml of $HgCl_2$, $Hg(NO_3)_2$ or $Hg(OAc)_2$ solutions. The kinetic points were collected after certain time intervals until the reaction mixture concentration remained unchanged. The aliquots volume of 25–50 μL were taken from adsorption containers to measure the residual concentrations until equilibrium attained. The amount of mercury removed was calculated from the difference between the initial and residual concentrations. The kinetic experiments were done in triplicate and the average standard deviation was below 5.2%. The amount of mercury removed was calculated from the difference between the initial and final solution concentrations.

2.4. Materials characterization and analytical methods

Fourier Transform Infrared Spectra (FTIR) were recorded on Agilent technologies, Cary 600 series FTIR spectrometer in transmission (T) mode at wavenumbers range 500–4000 cm^{-1} with a resolution of 2 cm^{-1}. The chemical composition of samples was determined on X–ray fluorescence (XRF) using an Axios Max (XRF, PANalytical) operating with Rh X-ray tube and four analyzing crystals, namely LiF200, PE002, PX1 and LiF220. The powder was then dispersed to retrieve X-ray diffraction (XRD) patterns on Rigaku (SmartLab® X-ray) diffraction system with Cu Kα radiation source (λ = 1.54 Å) at a scan rate of $0.02°\theta\bullet s^{-1}$. The morphological characteristics of samples were studied by Scanning Electron Microscopy (SEM) using a JEOL 6380LV, operating in LV mode, at 20 kV, equipped with a backscattered electron detector. The chemical mapping of samples were conducted using a Si (Li) Energy-Dispersive X-ray spectrometer (EDX, INCA X-sight, Oxford Instruments) connected to SEM. Transmission Electron Microscope (JEOL JEM-2100 LaB6) was used to examine the morphology and size of the formed silver nanoparticles. The mercury concentration in the aqueous samples was measured in triplication on a RA-915M Mercury Analyzer (Lumex-Ohio) with pyrolysis attachment (PYRO-915$^+$). The analysis of nitrates was done by ion chromatography using a Dionex ICS 6000/Aquion instrument.

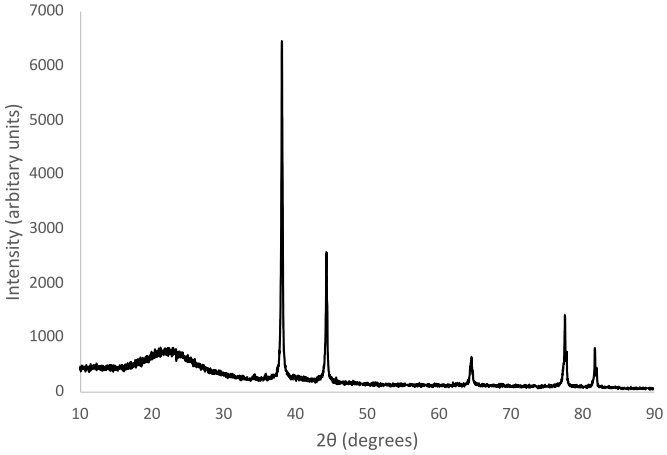

Fig. 2. XRD pattern of the Ag^0@SiO_2 sample.

3. Results and discussion

3.1. Materials characterization

The hydride content measured by iodometric titration was 0.06 ± 0.02 mmol/g for SiO2 and 0.75 ± 0.03 mmol/g for TES-SiO_2, which confirms successful modification of TES-SiO_2 with ≡ Si-H groups. The ≡ Si-H groups were detected in FTIR spectra at 2268 cm^{-1} (Fig. 1). The silver content measured by XRF was 55.9 mg/g. The XRD spectra are shown in Fig. 2. The peaks at 38.16°, 44.36°, 64.56° and 77.62° are characteristic of metallic Ag^0 (PDF card 0–001-1164). Using the Scherrer equation and the peak at 38.16° the size of Ag^0 NPs was estimated at 57 nm. The TEM images of Ag^0@SiO_2 samples clearly show spherical nanoparticles of variable sizes (Fig. 3), which is in a reasonable agreement with XRD results.

3.2. Mercury sorption kinetics

The % removal of mercury by the TES-SiO_2 and Ag^0@SiO_2 from the solutions is shown in Figs. 4–6. As is evident, TES-SiO_2 is superior in all solutions owing to the high reactivity of hydride ions. In Ag^0@SiO_2 case the maximum mercury uptake capacity followed the order $HgCl_2 \gg Hg(OAc)_2 > Hg(NO_3)_2$, while the removal rate the order $Hg(OAc)_2 \gg$

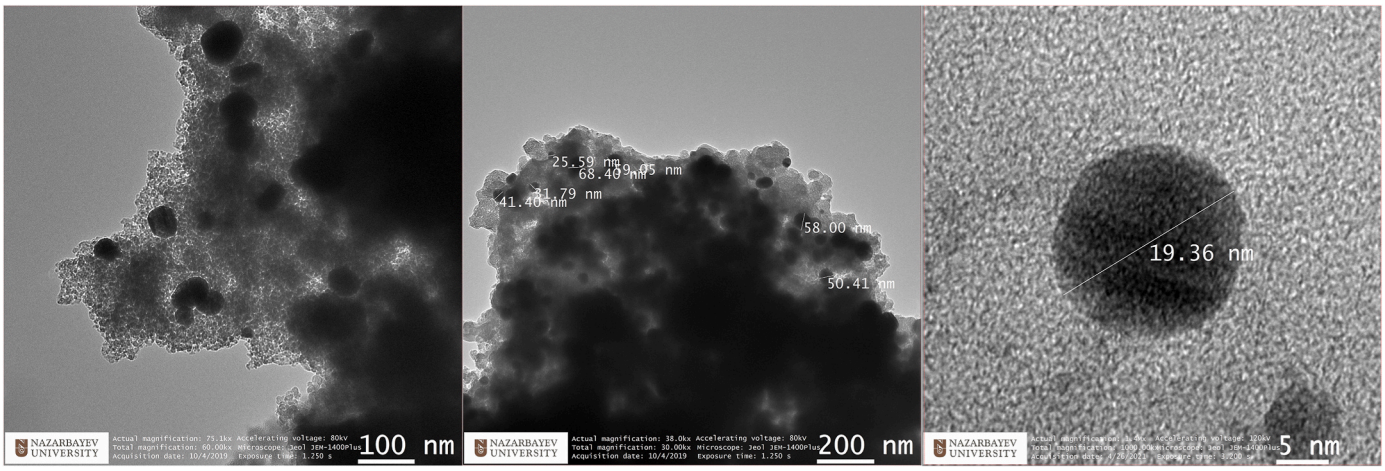

Fig. 3. Representative TEM images of the $Ag^0@SiO_2$ sample.

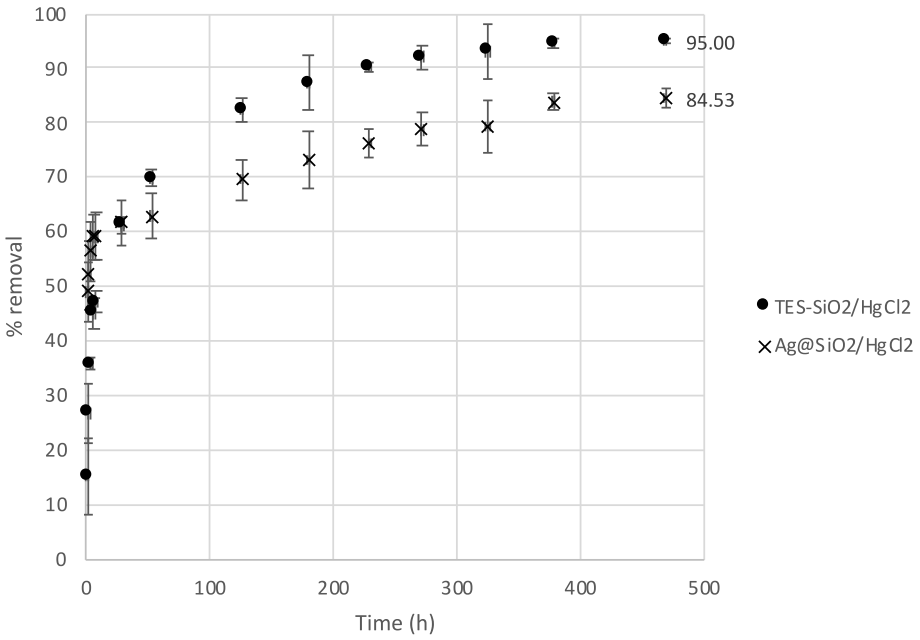

Fig. 4. Mercury uptake from the chloride solution.

$HgCl_2 > Hg(NO_3)_2$.

The XRD results are presented in Figs. 7–9. The rectangles highlight the main differences between the samples. For the chloride solution, TES-SiO_2 and $Ag^0@SiO_2$ samples showed peaks at 21.35°, 28.1°, 31.6°, 32.7°, 40.15°, 43.7°, 46.3°, 52.8° and 58.25°, which are characteristic of Hg_2Cl_2 (PDF card 00-001-0768). The $Ag^0@SiO_2$ samples showed additional peaks at 32.2°, 54.8° and 57.4° characteristic of AgCl (PDF card 00–001-1013). Also, it shows an additional peak at 39.4°, characteristic of schachnerite $Ag_{1.1}Hg_{0.9}$ (PDF card 00-027-0618). For the nitrate solution, TES-SiO_2 shows no new peaks while the $Ag^0@SiO_2$ samples showed peaks at 34.5°, 36.95° and 39.3°is characteristic of schachnerite $Ag_{1.1}Hg_{0.9}$. For the acetate solution, TES-SiO_2 shows no new peaks while the $Ag^0@SiO_2$ samples showed peaks at 38.1°, 44.2°, 44.2°, 64.6° and 77.6°, which are characteristic of Ag^0 and a peak at 39.6° which is characteristic of schachnerite $Ag_{1.1}Hg_{0.9}$. The same sample was measured after 7 days of interaction with the solution and the results showed only three peaks at 38°, which is characteristic of Ag^0 and 37.1° and 39.6°, which are characteristic of schachnerite $Ag_{1.1}Hg_{0.9}$. This indicates that even after the uptake of mercury is completed the silver is further oxidized and the amalgam formation evolves, a phenomenon that requires further research.

The TEM samples of the $Ag^0@SiO_2$ show dark spots and mostly absence of well defined spherical Ag^0 nanoparticles (see Fig. 10). The SEM-EDS clearly shows the coexistence of Hg and Ag with Cl in samples interacted in chloride solutions and Ag and Hg in samples interacted in nitrate solutions. In in samples interacted in acetate solutions no such coexistence was observed, probably because of the small size of formed amalgam particles.

3.3. Interaction mechanisms

3.3.1. Interaction of metals with SiO_2

Silanol groups are weakly acidic and as pH increases above 2 ± 1 the silica surface develops a net negative charge primarily due to deprotonation (Lowe et al., 2015; Wu and Lin, 2013; Zienkiewicz-Strzałka et al., 2018):

$$\text{-SiOH} \rightleftharpoons \text{-SiO}^- + H^+ \quad (5)$$

The potential interactions of metals with the surface of SiO_2 are adsorption and ion exchange. Dugger et al. (1964) and Mustafa et al.

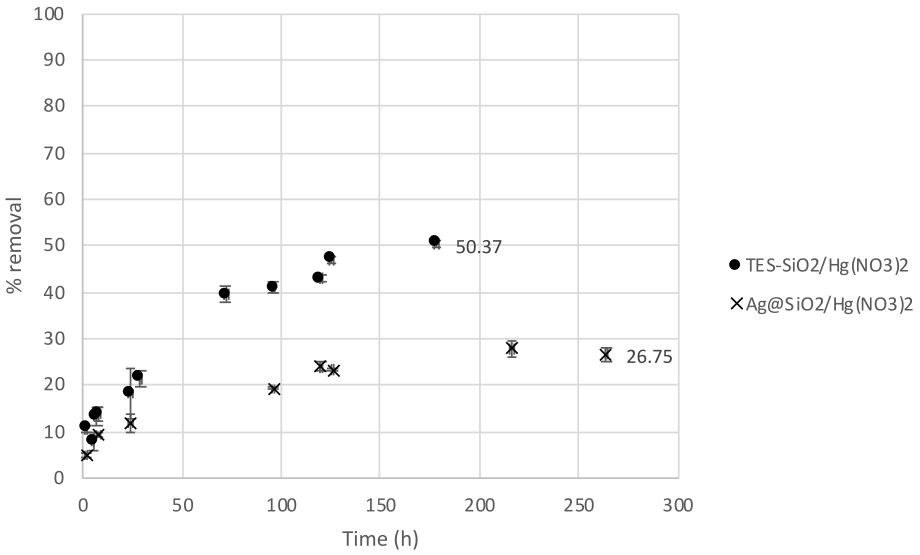

Fig. 5. Mercury uptake from the nitrate solution.

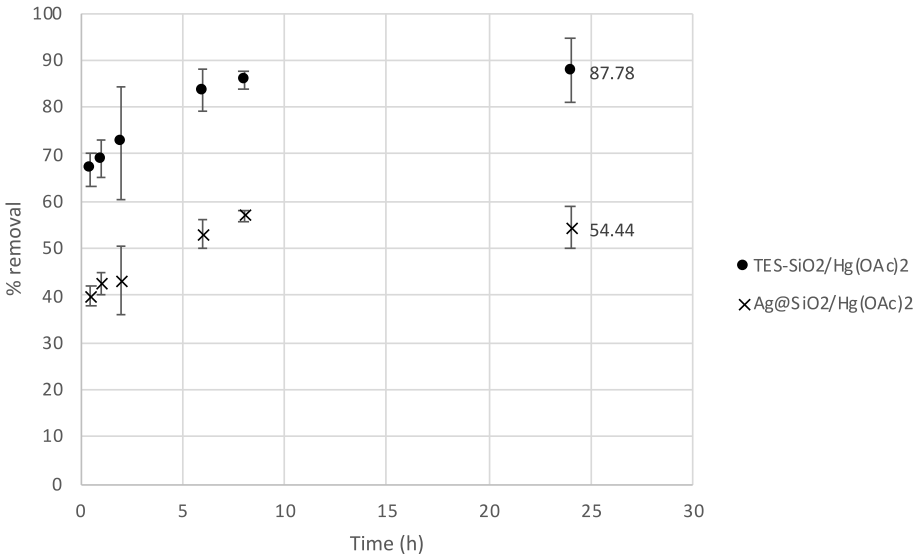

Fig. 6. Mercury uptake from the acetate solution.

(2003) studied the exchange of several metals ions on silica gel and an ion exchange mechanism between cations and hydrogen ions was proposed:

$$m(\text{-SiO}^-)H^+ + M^{m+} \rightleftharpoons (\text{-SiO})_mM + mH^+ \quad (6)$$

Ion exchange can happen at pH above 2 so deprotonation of silanol groups to happen and below a certain pH so free metal ions in the solution exist (Fig. 12). Katok et al. (2013) who found that amorphous (fumed) silica showed no affinity for mercury in $Hg(NO_3)_2$ solutions at pH 4 and low concentration (1.4 ppm). The explanation provided is that only 0.1% of silanol groups are ionized at this pH and thus cation exchange between Hg^{2+} and H^+ is not possible. Belyakova et al. (2009) used amorphous silica (C-120) to study the removal of Hg^{2+} from nitrate solutions at pH near to 1 and argued that silanol group ionization is negligible below pH 4.5 and the removal of Hg^{2+} is insignificant as cation exchange cannot happen. However, a closer look at the results reveals that this is true for low concentrations but at initial concentration of 1000 ppm the loading reached about 20 mg/g, which is clearly not insignificant.

Other studies reported that ion exchange is not significant in comparison to adsorption. Surface complexation and formation of bonds between metals and oxygen atoms on the surface of silica were described as the adsorption mechanism for the removal of Hg^{2+} from low concentration solutions (ppb level) and pH above 2 by α-SiO_2 (Tiffreau et al., 1995). Adsorption OH^- and Cl^- complexes can explain the uptake of Hg^{2+}. The same mechanisms were discussed by Bonnissel-Gissinger et al. (1999) who studied the adsorption of Hg^{2+} on amorphous silica (Aerosil 200) in low concentrations (2.48 ppm). The mechanism was described as adsorption of OH^- and Cl^- complexes rather than ion exchange of free Hg^{2+} ions. Etale et al. studied the removal of mercury in the absence of Cl^- by use of commercial silica at low concentrations (<1.53 ppm) and observed that positively charged mercury species at pH 3 are not adsorbed while mercury removal increased in higher pH due to the adsorption of $Hg(OH)_2$ complexes (Etale et al., 2014). In this study, blank experiments with SiO_2 showed 0.4%, 1.9% and 6% average removal of mercury from acetate, chloride and nitrates solution, respectively. Ion exchange should happen at low pH as free Hg^{2+} ions exist in the solution and silanol groups are ionized and adsorption follows at higher pH values. However, the mercury uptake is either very

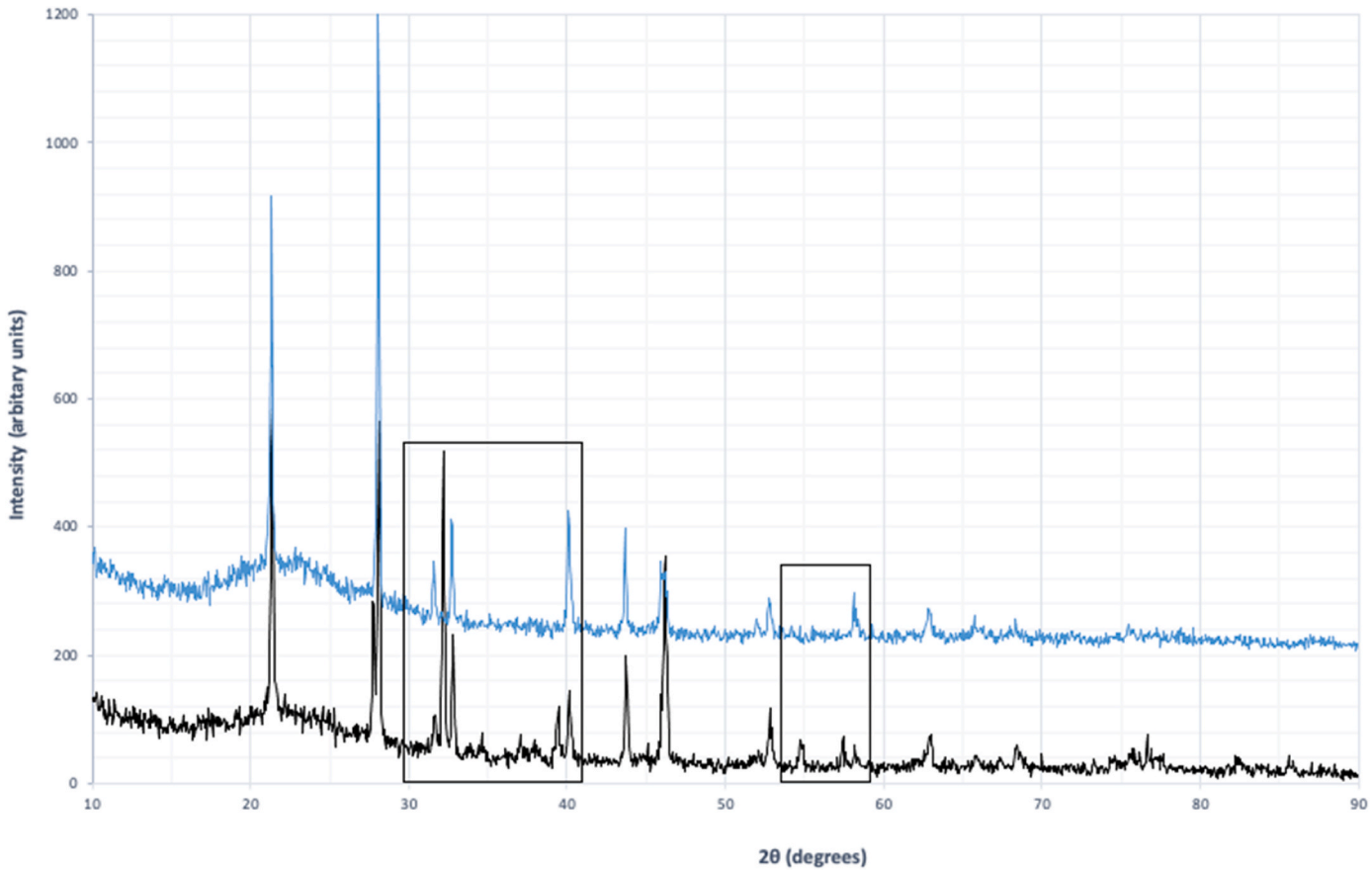

Fig. 7. XRD analysis of TES-SiO_2 (top) and Ag^0@SiO_2 (bottom) samples after mercury adsorption from chloride solution.

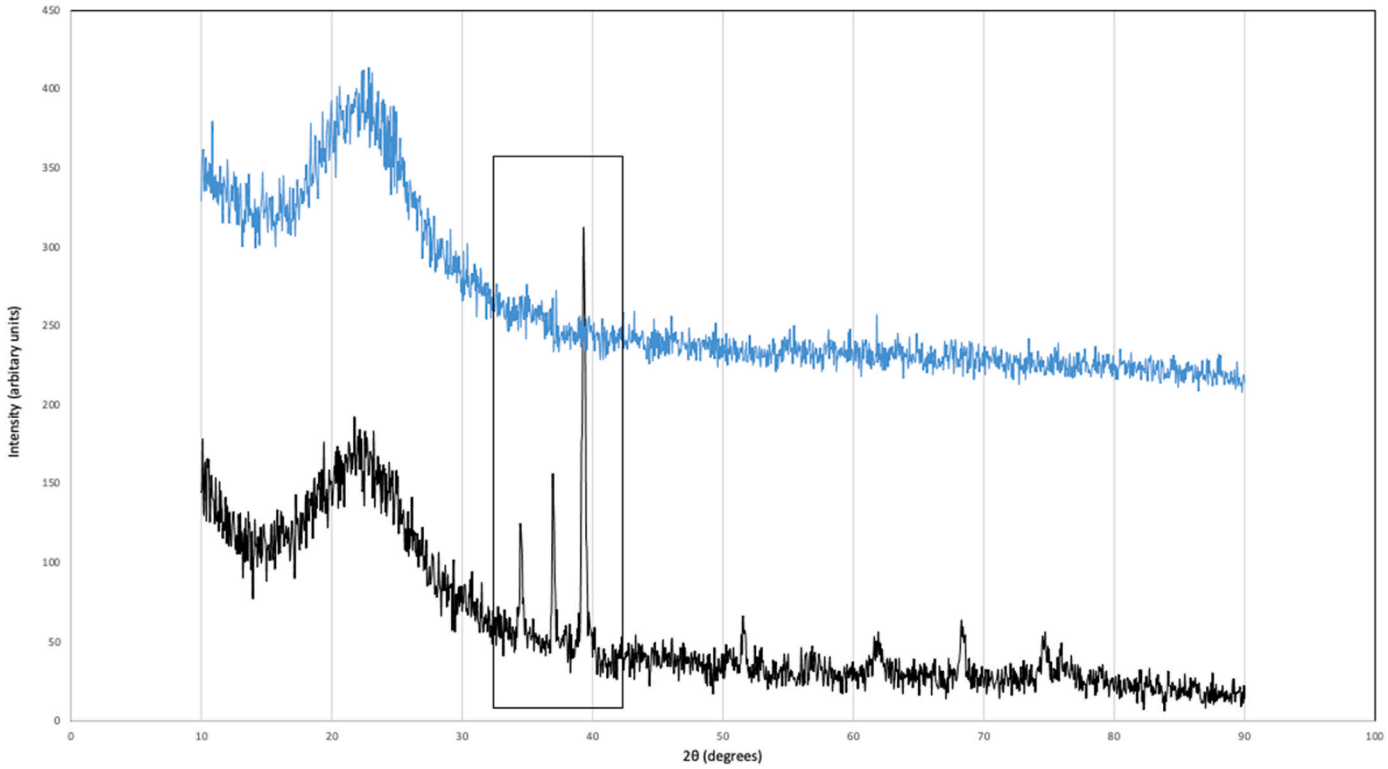

Fig. 8. XRD analysis of TES-SiO_2 (top) and Ag^0@SiO_2 (bottom) samples samples after mercury adsorption from nitrates solution.

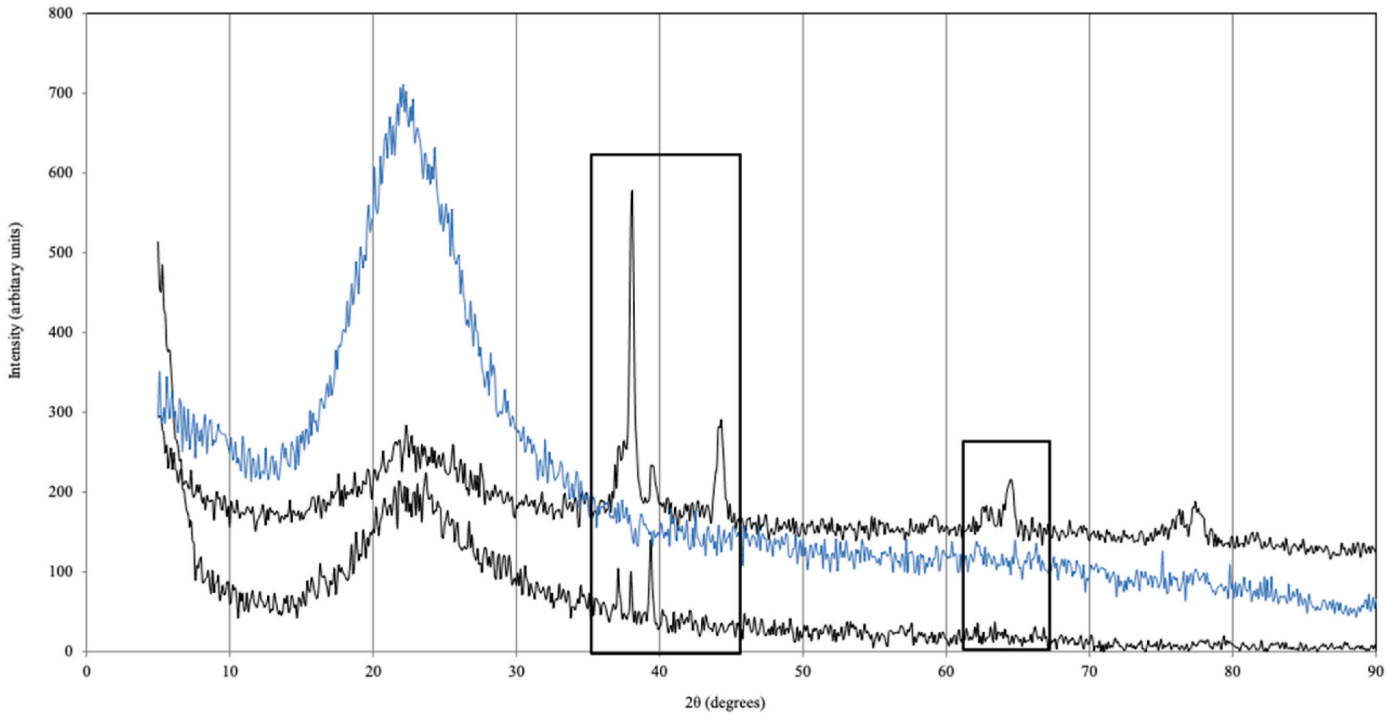

Fig. 9. XRD analysis of TES-SiO_2 (top), Ag^0@SiO_2 (middle) and Ag^0@SiO_2 after 7 days (bottom) samples samples after mercury adsorption from acetate solution.

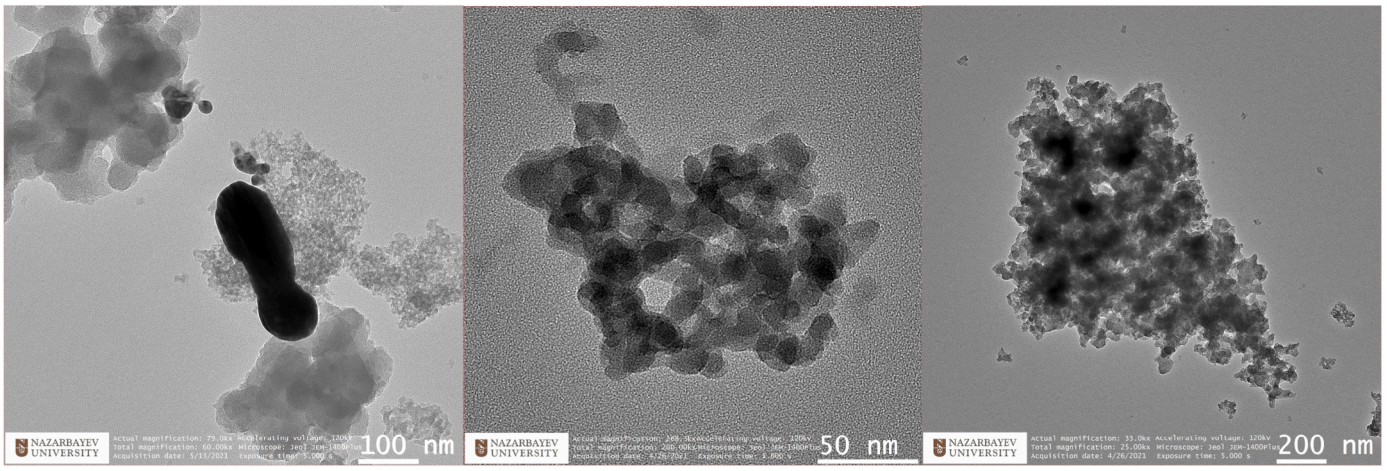

Fig. 10. Representative TEM images of the Ag^0@SiO_2 samples after mercury sorption.

low or insignificant.

3.3.2. *Silicon hydride reaction with metals*

The reaction between SiO_2 and TES can be represented as follows (Katok et al., 2013):

$$3(-SiOH) + (OCH_2CH_3)_3SiH \rightarrow [3(-SiO)]SiH + 3CH_3CH_2OH \quad (7)$$

The silicon in the silicon-hydrogen bonds formed on silica surface after TES modification is more positive than hydrogen and therefore the hydrogen atom bears a negative charge and can be eliminated as a hydride ion (Katok et al., 2013). The reaction in water is favored in alkaline solutions (Katok et al., 2013):

$$-SiH + H_2O \rightarrow -SiOH + H^- + H^+ \quad (8)$$

The hydride ion reacts with the proton from water to form hydrogen. Considering that the reduction potential of the hydride ion is much lower than most of metals (Table 1) H^- can be oxidized to form hydrogen with a simultaneous reduction of the metal which is adsorbed on the surface of the solid (Katok et al., 2013). The reactions of interest can be found in literature and are adapted here to better depict the mechanisms and stoichiometry (Katok et al., 2012, 2013; Reed-Mundell et al., 1995):

$$2(-SiH) + 2Hg^{2+} + 2H_2O \rightarrow [2(-SiO)]Hg_2^{2+} + 4H^+ + H_2(g) \quad (9)$$

$$-SiH + Ag^+ + H_2O \rightarrow \left(-SiOAg^0\right) + H^+ + 0.5H_2(g) \quad (10)$$

The solution pH plays an important role on mercury removal as it can influence the aqueous phase speciation, the stability of the silicon hydride groups and the deprotonation of silanol groups. In the published studies it is not clear how the Hg_2^{2+} and Ag^0 are anchored on the surface of SiO_2. It seems plausible that Hg^{2+} and Ag^+ are first electrostatically attracted by the negative ($-SiO^-$) groups where the reduction that follows bounds them on the surface:

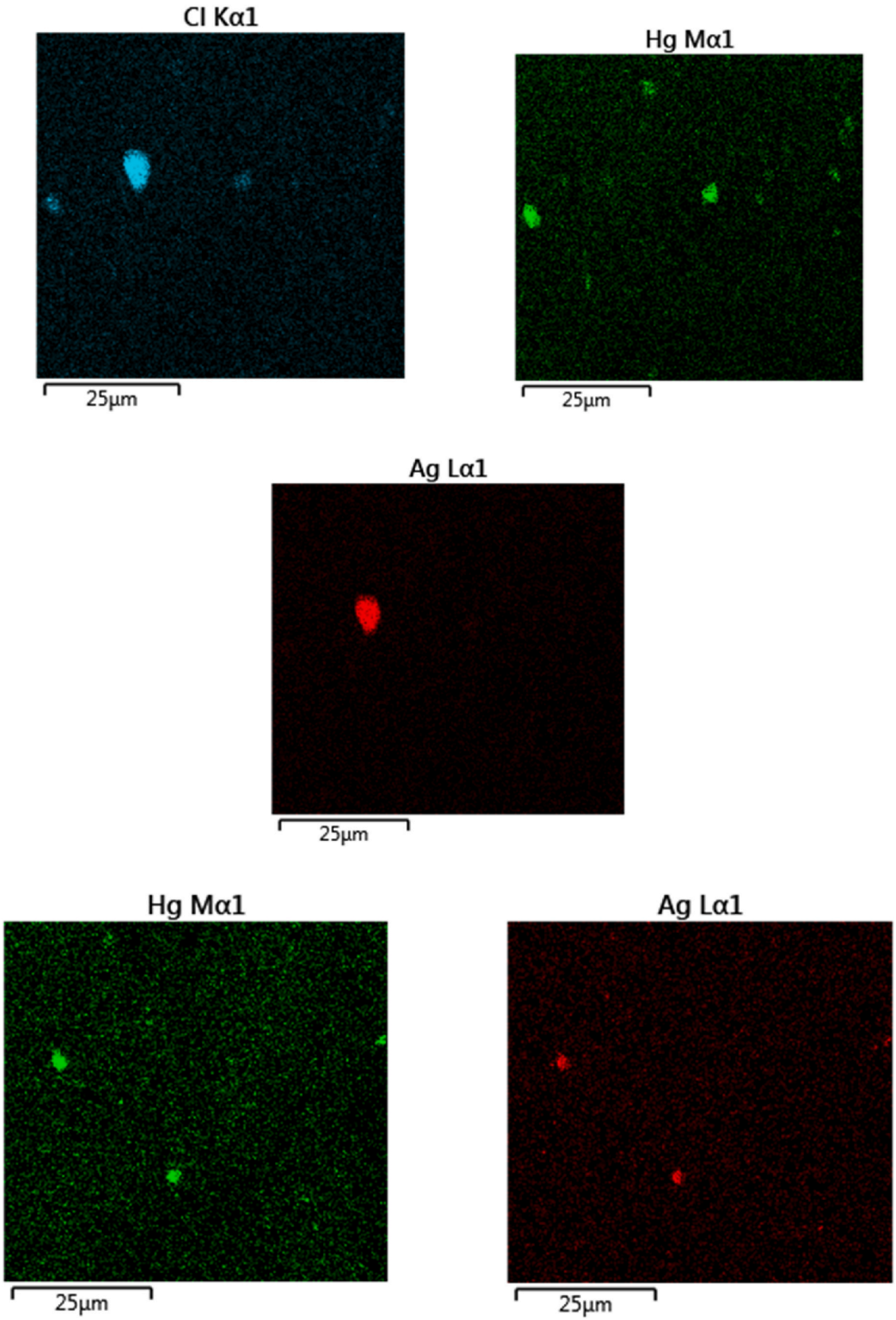

Fig. 11. SEM-EDS images of the Ag^0@SiO_2 samples after mercury sorption in chloride (top), nitrate (middle) and citrate (bottom) solutions.

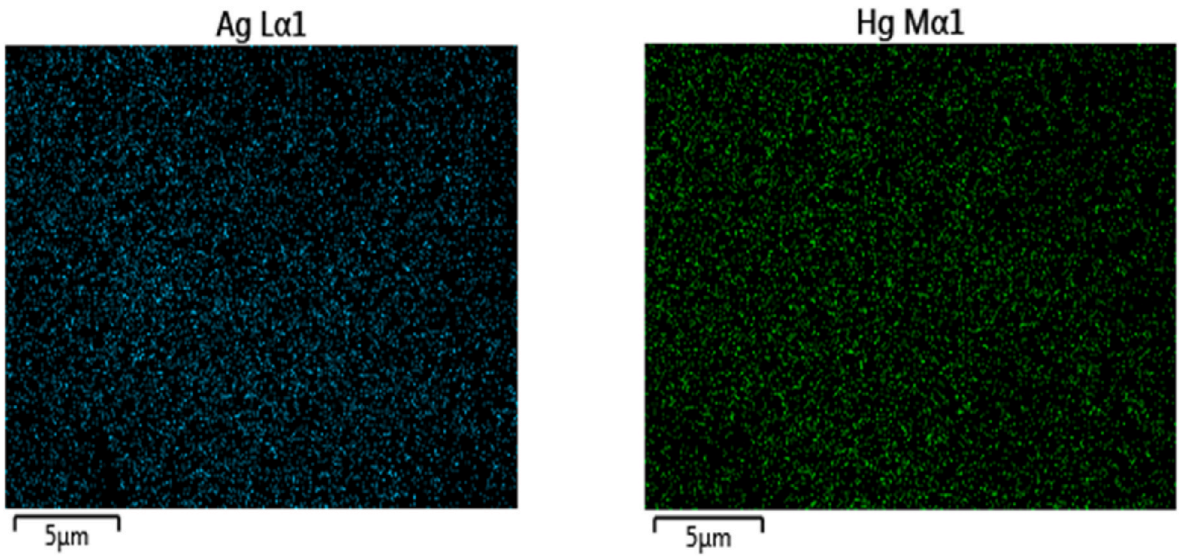

Fig. 11. (*continued*).

$$-SiH + Ag^{+} + H_2O \rightarrow (-SiO^{-})Ag^{+} + H^{-} + 2H^{+} \quad (11)$$

$$(-SiO^{-})Ag^{+} + H^{-} \rightarrow -SiOAg^{0} + 0.5H_2 \quad (12)$$

However, as it is discussed above, in the pH range of 2–4.5 the surface is only slightly negative and control experiments with unmodified SiO_2 showed that this electrostatic attraction does not seem sufficient to result in significant uptake of Hg^{2+}. Nevertheless, negative metals species can follow the same general reaction scheme, as for instance the interaction of $PtCl_6^{2-}$ with the surface of silica and the anchoring of Pt^0 on its surface (Tertykh et al., 2013).

3.3.3. Silver interaction with mercury

Due to the dissolved oxygen in the solution Ag^0 is oxidized:

$$2Ag^0 + 0.5O_2 \rightarrow Ag_2O \quad (13)$$

This reaction should be slow enough to allow reducing conditions to form locally on the SiO_2 surface and reactions (1) and (2) to take place. As it will be discussed, in contrast to Katok et al. (2012), in this study it is assumed that both Hg_2^{2+} and Hg^0 are formed although the Hg^0/Hg_2^{2+} ratio is not known. The co-existence of Ag^0 and Hg^0 results in amalgamation, which in the presence of Cl^- is accompanied by calomel precipitation:

$$0.9Hg^0 + 1.1Ag^0 \rightarrow Ag_{1.1}Hg_{0.9} \quad (14)$$

$$Hg_2^{+2} + 2Cl^{-} \rightarrow Hg_2Cl_2 \quad (15)$$

Finally, the dissolution of Ag_2O takes place (Tauanov et al., 2020) which allows the formation of AgCl:

$$Ag_2O + 2H^{+} \rightarrow 2Ag^{+} + H_2O \quad (16)$$

$$Ag^{+} + Cl^{-} \rightarrow AgCl \quad (17)$$

Amalgamation (reaction 14) is expected to be slower than the precipitation reaction (15) due to (a) possible the stepwise partial reduction of Hg^{2+} via Hg_2^{2+}, (b) the slow diffusion of Hg^0 though the Ag^0/amalgam layers and (c) the stoichiometry. The reduction of 1 mol of Hg^{2+} to Hg_2^{2+} and the formation of calomel requires in total 1 mol of Ag^0 (Hg:Ag molar ratio of 1) while the reduction of 1 mol of Hg^{2+} to Hg^0 and the formation of amalgam requires in total 3.22 mol of Ag^0 (Hg:Ag molar ratio of 0.31) (Azat et al., 2020). This means that regardless the reactions rate, for the same amount of Ag^0 on SiO_2, amalgamation is expected to result in lower Hg^{2+} uptake than precipitation (reaction 15), which agrees with the experimental results (Figs. 4–6). For more details of the diffusion

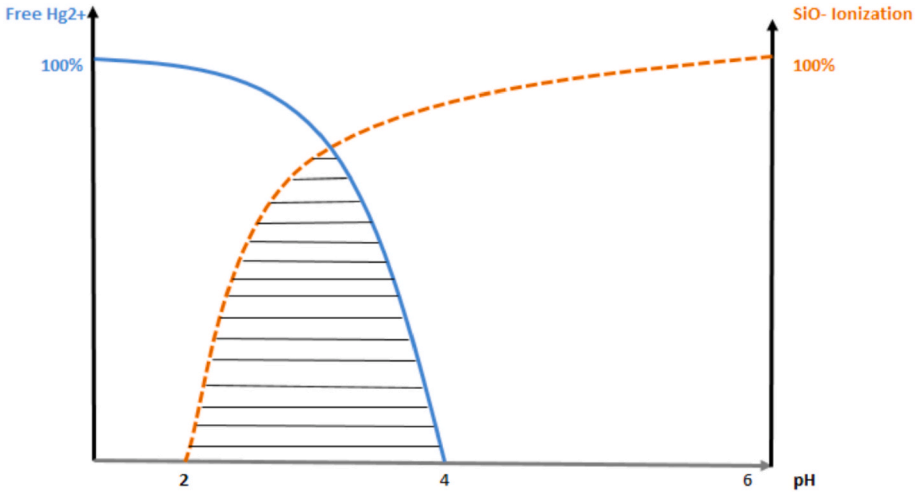

Fig. 12. Qualitative representation of the conditions where ion exchange can take place.

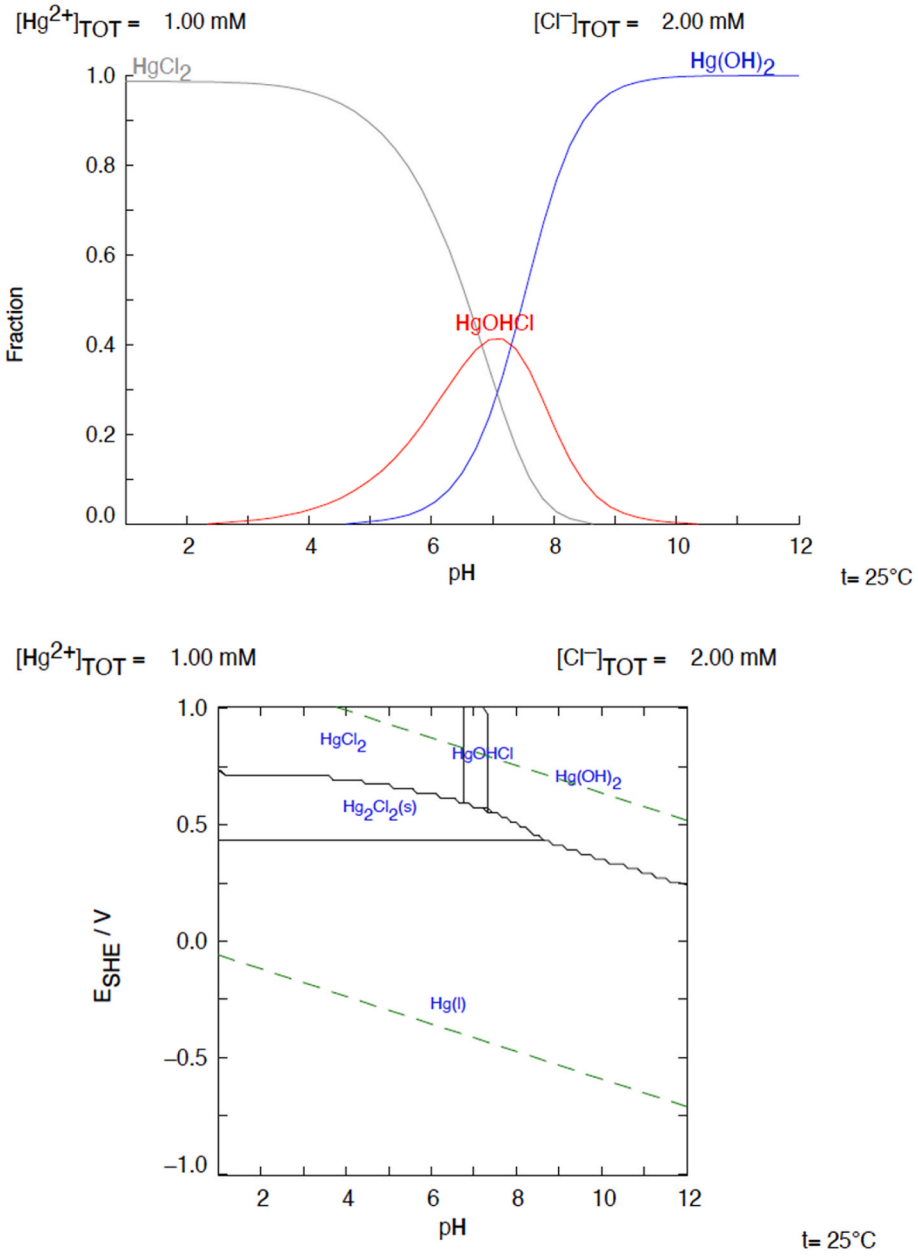

Fig. 13. Speciation (upper, middle) and Pourbaix (lower) diagrams for $HgCl_2$ solutions.

phenomena during Ag-Hg amalgamation see Liu and Huang (2013).

3.3.4. The effect of aqueous phase chemistry

To better understand the surface reaction mechanisms taking place on TES-SiO_2 and Ag^0@SiO_2, the mercury speciation in Fig. 7 and the Pourbaix diagram in Fig. 8 at a concentration of 200 ppm of Hg^{2+} are presented for the three studied systems. All diagrams were created by using Medusa software. It is important to mention that the lines in the Pourbaix diagram represent the E_{SHE}-pH conditions where, in equilibrium, the content of the adjacent species is the same. However, these species always exist in smaller amounts on both sides of these lines and may influence the properties of the systems. For the discussion that follows the assumption is that the chemical speciation represents the mercury species in the solution while the Pourbaix diagram the redox products on the surface of SiO_2. Thus, redox reactions were included in modeling for the Pourbaix diagrams but not for the speciation diagrams. The formation of HgO, an orange-red precipitate, is possible but is excluded from modeling as no precipitate was observed under the experimental conditions studied.

3.3.4.1. $HgCl_2$ solutions. In $HgCl_2$ solutions and over the observed pH range (3.6–4.4) only neutral $HgCl_2$ is formed in the solution and the reduction of Hg^{2+} in a complex is expected to be more difficult than this of free Hg^{2+}. The surface reduction of Hg^{2+} (reactions 1 and 2) drives the system in the Hg_2^{2+} predominance area (reaction 15), coexisting with some Hg^0 (Fig. 13). Further reduction of Hg_2Cl_2 to Hg^0 can only happen in TES-SiO_2 system, as hydride reduction potential is lower than this of calomel (Table 1). In Ag^0@SiO_2 system, the presence of Hg^0 leads to the formation of Ag-Hg amalgams (reaction 14). Also, from Table 1 is clear that hydride reduction potential is much lower than this of Ag^0 and thus it can more effectively reduce mercury ions (reaction 9). The formation of Hg_2Cl_2 in both TES-SiO_2 and Ag^0@SiO_2 and AgCl and $Ag_{1.1}Hg_{0.9}$ in Ag^0@SiO_2 is clear in XRD spectra (Fig. 7). Also, the formation of Hg_2Cl_2 and AgCl in Ag^0@SiO_2 is evident in SEM-EDS analysis (Fig. 11).

3.3.4.2. $Hg(NO_3)_2$ solutions. In $Hg(NO_3)_2$ solutions and over the

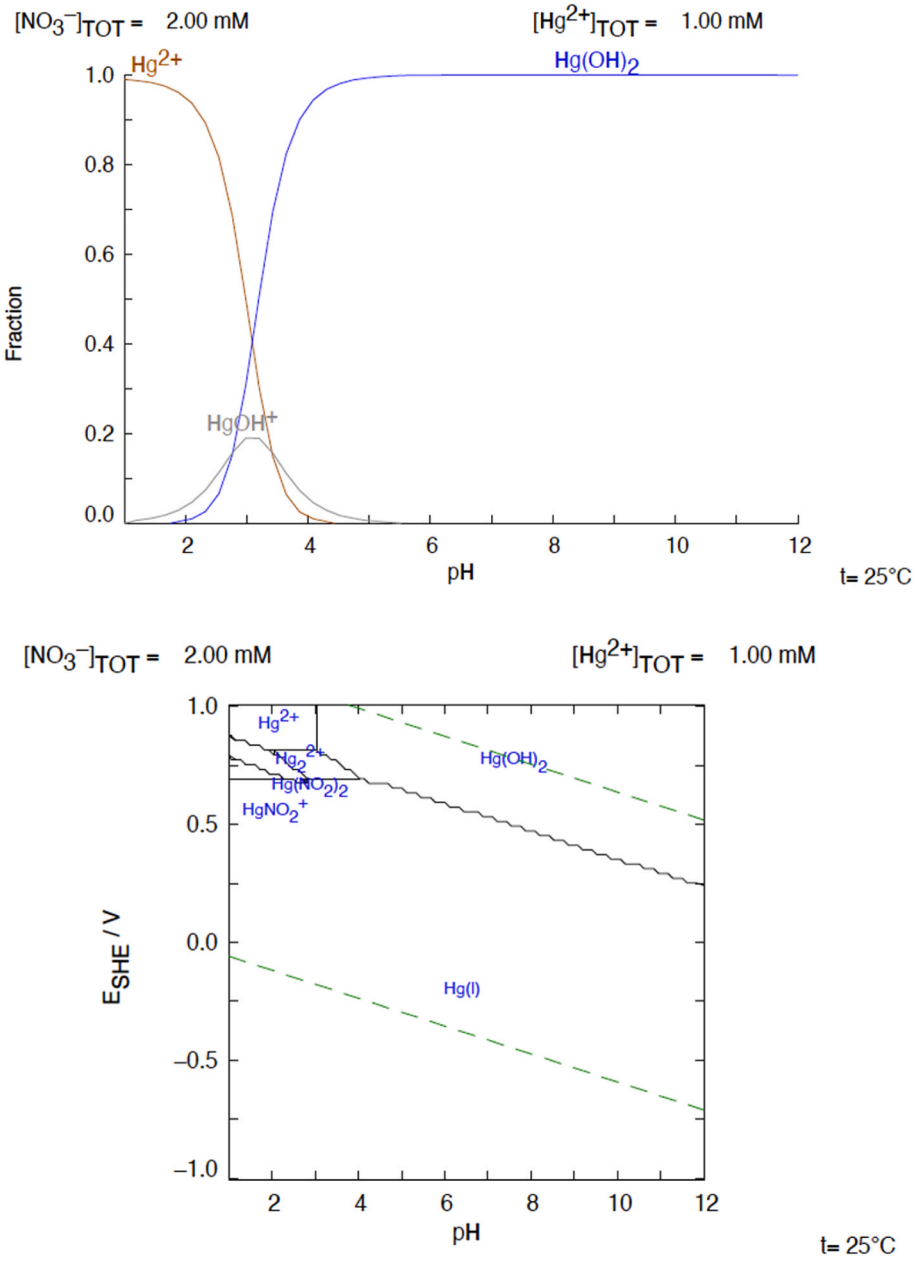

Fig. 14. Speciation (upper, middle) and Pourbaix (lower) diagrams for $Hg(NO_3)_2$ solutions.

observed pH range (2.3–4) Hg^{2+} coexists with stable $Hg(OH)_2$ complexes and the surface reduction drives the system in the Hg_2^{2+} predominance area, coexisting with some Hg^0 (Fig. 14). Further reduction of Hg_2^{2+} to Hg^0 can only happen in TES-SiO_2 system, as silver ion and mercuric ion reduction potentials are practically equal (Table 1). However, Hg^0 was not detected on the surface of TES-SiO_2 by Katok et al. (2013), who worked at pH around 4. In Ag^0@SiO_2 system, the presence of Hg^0 leads to the formation of Ag-Hg amalgams (reaction 14). The formation of $Ag_{1.1}Hg_{0.9}$ in Ag^0@SiO_2 is clear in XRD spectra (Fig. 8) and SEM-EDS analysis (Fig. 11)

Being predominate species, the adsorption of Hg_2^{2+} on silver cannot be excluded. The pH gradually increases during the reaction reaching about 3.5–4 at its completion in all studied solutions. The removal of Hg^{2+} from the solution tends to increase the pH and reaction (3), for TES-SiO_2 and (7) for Ag^0@SiO_2 tends to decrease the pH. After interaction with mercury, in TES-SiO_2 solutions the pH was lower than in Ag^0@SiO_2 solutions by 0.2–0.65. This is an advantage for TES-SiO_2 system as the amount of free Hg^{2+} ions is higher.

Katok et al. (2012) discussed on the possibility a redox active anion, such as nitrate and acetate, to facilitate the reduction of silver released into solution under conventional redox chemistry and allow silver to partake in further reduction of mercury. The reactions they provide are:

$$Hg^{2+} + 2NO_3^- + H_2O \rightarrow Hg^0 + 2H^+ + 2NO_2^- + 1.5O_2 \quad (18)$$

$$Hg^{2+} + 2NO_3^- + H_2O \rightarrow Hg^0 + 2HNO_2 + 1.5O_2 \quad (19)$$

Although thermodynamically favorable the rate of these reactions is not known (Katok et al., 2012). A different and more likely hypothesis is based on the reduction potential of nitrate (Table 1). The reduction of nitrates by inorganic materials has been reviewed by Zhu and Getting (2012) and Fanning (2000). Several metals such as Fe, Cu, Zn and Pb can reduce nitrates to ammonium in acidic conditions. Kang et al. studied the reduction of nitrate to ammonium by bimetallic Fe/Ni nanoparticles (Kang et al., 2012). In the case of TES-SiO_2 nitrate can oxidize hydride and hinder the uptake of Hg^{2+}. In the case of Ag^0@SiO_2 the nitrates

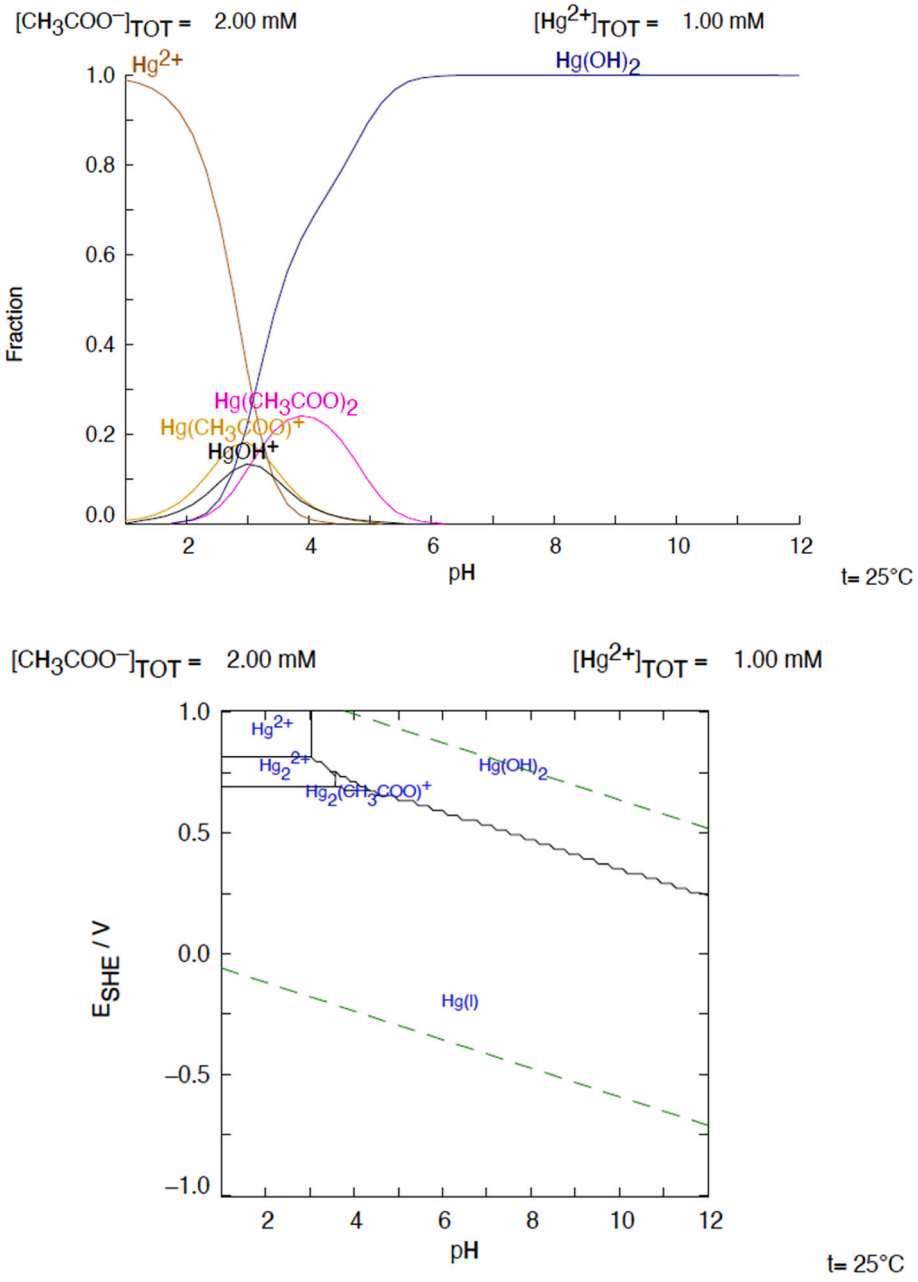

Fig. 15. Speciation (upper, middle) and Pourbaix (lower) diagrams for $Hg(OAc)_2$ solutions.

reduction potential to NH_4^+ or N_2 is higher than Ag^0, Hg_2^{2+} and Hg^0 causing their oxidation and hindering the formation of amalgams. To validate this hypothesis the nitrates concentration in $Hg(NO_3)_2$ solutions were measured. The results showed a considerable decrease of nitrates by approximately 65% in both TES-SiO_2 and Ag^0@SiO_2 solutions. The concentration of nitrates is constant after 8h and up to 264h. The stock solution theoretical nitrates concentration was 124 ppm and the colorimetric method showed 98 ± 4 ppm. Despite the modest accuracy of the method, the decrease of nitrates concentration in both TES-SiO_2 and Ag^0@SiO_2 is firmly confirmed and thus there is a strong indication of nitrates reduction.

3.3.4.3. $Hg(OAc)_2$ solutions. The observed pH range of the is (2.5–4.1), similar to this of $Hg(NO_3)_2$ solutions. Again, the surface reduction (reactions 1 and 2) drives the system in the Hg_2^{2+} predominance area, coexisting with some Hg^0 (Fig. 15) and further reduction of Hg_2^{2+} to Hg^0 can only happen in TES-SiO_2 system. In Ag^0@SiO_2 system, Ag-Hg amalgamation is more pronounced indicating that the amount of formed Hg^0 is higher than in $Hg(NO_3)_2$ solution. This agrees with Katok et al. (2012) who found that the amalgamation reaction in $Hg(OAc)_2$ solution is more efficient. Also, given its relatively high amount, adsorption of Hg_2^{2+} on silver cannot be excluded. Although SEM-EDS analysis shows no amalgam (Fig. 11) the XRD spectra clearly shows the formation of $Ag_{1.1}Hg_{0.9}$ in Ag^0@SiO_2 (Fig. 9) but there is no evidence of amalgam in SEM-EDS analysis.

In the case of TES-SiO_2 acetate can oxidize hydride and reduce Hg^{2+} but the oxidation effect is more pronounced in the presence of nitrates as its reduction potential is much higher than this of acetate (Table 1). In the case of Ag^0@SiO_2 the acetate reduction potential is lower than this of both Ag^0 and Hg^0 and thus it can contribute to the reduction enhancing the reaction rate of amalgams. Thus, in both systems the mercury removal from $Hg(OAc)_2$ solution is expected higher in comparison to $Hg(NO_3)_2$ solution. Finally, as Cl^- is stable (Table 1), and there is no such effect as this of nitrates and acetate in $HgCl_2$ solution.

3.3.4.4. Interactions molar ratios. The estimated H:Hg molar ratio in TES-SiO_2 samples is 0.33–0.66 close to this observed for a similar material by Katok et al. (2013) (0.40–0.56) and Inglezakis et al. (2021) (0.52). Obviously, this is considerably lower than the stoichiometry of the reaction (3) however this can be explained by considering the hydrolysis of hydride according to reaction (1) resulting in less available hydride for reduction. Assuming that all Ag^0 reacts the Hg:Ag molar ratio in $Hg(OAc)_2$ solution is 0.53, higher than the stoichiometric expected for the redox reaction and the formation of amalgam, an evidence of hyperstoichiometry, reported only once so far by Katok et al. (2012). This result however requires further verification as acetate can contribute to the reduction of Hg^{2+} while adsorption of Hg^{2+} and Hg_2^{2+} on the surface of silica cannot be excluded. The Hg:Ag molar ratio in $Hg(NO_3)_2$ (0.25) and $HgCl_2$ (0.83) solutions are lower than the stoichiometric but considering the large nanoparticles size observed in this study (57 nm) is in agreement with the published data which show scaling of stoichiometry with the nanoparticle size.

4. Conclusions

In this study, the direct nanoscale Ag-Hg amalgamation on the surface of amorphous silica was investigated. The findings show that the presence of chloride (Cl^-), acetate (OAc^-), and nitrate (NO_3^-) ions in the solution significantly influence the mercury removal process. Mercury uptake capacity followed the order $HgCl_2 > Hg(OAc)_2 > Hg(NO_3)_2$, while the reaction rate the order $Hg(OAc)_2 > HgCl_2 > Hg(NO_3)_2$. The formed amalgam was $Ag_{1.1}Hg_{0.9}$ in all solutions while and the presence of chloride ions (Cl^-) led to the co-formation of Hg_2Cl_2 and AgCl alongside the amalgam. The results demonstrate the potential of the $Ag@SiO_2$ nanocomposite for the removal of Hg^{2+} and the effect of the anions which drastically alter the mercury speciation and the surface redox reactions. The estimated Hg:Ag molar ratio in $Hg(OAc)_2$ solution was found higher than the stoichiometric expected for the redox reaction and the formation of the amalgam, an evidence of hyperstoichiometry. While this result is groundbreaking it requires further verification using advanced surface analysis characterization. The specific form of mercury present in water affects the effectiveness of various removal technologies and, consequently, the success of remediation efforts. Furthermore, the presence of anions in water plays a vital role in mercury complexation, altering the aqueous mercury species charge. This distinction is crucial because remediation methods effective for ionic mercury, such as ion exchange resins and zeolites, prove ineffective when mercury exists as neutral complexes. In such cases, adsorption emerges as the preferred removal strategy. Notably, redox interactions involving silver demonstrate efficacy across both ionic and neutral mercury forms, rendering this approach more adaptable and efficient compared to other materials and methods. In terms of applications these findings are of particular importance in water remediation and treatment as the synthesized materials are sustainable and can remove mercury from water effectively. Also, the results offer insights on the effects of mercury speciation on the removal performance which is of crucial importance and fills a gap in the related literature.

CRediT authorship contribution statement

V.J. Inglezakis: Writing – original draft, Visualization, Validation, Supervision, Software, Resources, Project administration, Methodology, Investigation, Funding acquisition, Formal analysis, Data curation, Conceptualization. **S. Azat:** Methodology, Conceptualization. **N. Kinayat:** Investigation. **A. Guney:** Investigation. **Z. Baimenova:** Investigation. **Z. Tauanov:** Writing – review & editing, Methodology, Investigation, Funding acquisition.

Declaration of competing interest

No conflict of interest exists.

Acknowledgements

This work was financially supported by the Grant Number 110119FD4536 funded by Nazarbayev University and the Grant No. BR24992814 and AP14869646 funded by the Science Committee of the Ministry of Science and Higher Education of the Republic of Kazakhstan.

Data availability

No data was used for the research described in the article.

References

Azat, S., Arkhangelsky, E., Papathanasiou, T., Zorpas, A.A., Abirov, A., Inglezakis, V.J., 2020. Synthesis of biosourced silica-Ag nanocomposites and amalgamation reaction with mercury in aqueous solutions. Compt. Rendus Chem. 23, 77–92. https://doi.org/10.5802/crchim.19.

Azat, S., Korobeinyk, A.V., Moustakas, K., Inglezakis, V.J., 2019. Sustainable production of pure silica from rice husk waste in Kazakhstan. J. Clean. Prod. 217. https://doi.org/10.1016/j.jclepro.2019.01.142.

Azmi, A.A., Izzati Daud, A., Khairul, W.M., Hamzah, S., Wan Mohd Khalik, W.M.A., Hanis Hayati Hairom, N., 2023. Silica–silver core–shell nanoparticles incorporated with cellulose filter paper as an effective colorimetric probe for mercury ion detection in aqueous media: experimental and computational evaluations. Environ. Nanotechnol. Monit. Manag. 19. https://doi.org/10.1016/j.enmm.2022.100762.

Belyakova, L.A., Shvets, O.M., Lyashenko, D.Y., 2009. Formation of the nanostructure on a silica surface as mercury(II) ions adsorption sites. Inorg. Chim. Acta. 362, 2222–2230. https://doi.org/10.1016/j.ica.2008.10.004.

Bonnissel-Gissinger, P., Alnot, M., Lickes, J.P., Ehrhardt, J.J., Behra, P., 1999. Modeling the adsorption of mercury(II) on (hydr)oxides II: α-FeOOH (goethite) and amorphous silica. J. Colloid Interface Sci. 215, 313–322. https://doi.org/10.1006/jcis.1999.6263.

Bratsch, S.G., 1989. Standard electrode potentials and temperature coefficients in water at 298.15K. J. Phys. Chem. Ref. Data 18, 1–21.

Deng, L., Ouyang, X., Jin, J., Ma, C., Jiang, Y., Zheng, J., Li, J., Li, Y., Tan, W., Yang, R., 2013. Exploiting the higher specificity of silver amalgamation: selective detection of mercury(II) by forming Ag/Hg amalgam. Anal. Chem. 85, 8594–8600. https://doi.org/10.1021/ac401408m.

Dugger, D.L., Stanton, J.H., Irby, B.N., McConnelj, B.L., Cummings, W.W., Maatman, R.W., 1964. The exchange of twenty metal ions with the weakly acidic silanol group of silica gel. J. Phys. Chem. 68, 757–760. https://doi.org/10.1021/j100786a007.

Etale, A., Yalala, B., Tutu, H., Drake, D.C., 2014. Adsorptive removal of mercury from acid mine drainage: a comparison of silica and maghemite nanoparticles. Toxicol. Environ. Chem. 96, 542–554. https://doi.org/10.1080/02772248.2014.976223.

Fan, Y., Liu, Z., Wang, L., Zhan, J., 2009. Synthesis of starch-stabilized Ag nanoparticles and Hg2+recognition in aqueous media. Nanoscale Res. Lett. 4, 1230–1235. https://doi.org/10.1007/s11671-009-9387-6.

Fanning, J.C., 2000. The chemical reduction of nitrate in aqueous solution. Coord. Chem. Rev. 199, 159–179. https://doi.org/10.1016/s0010-8545(99)00143-5.

Ganzagh, M.A.A., Yousefpour, M., Taherian, Z., 2016. The removal of mercury (II) from water by Ag supported on nanomesoporous silica. J Chem Biol 9, 127–142. https://doi.org/10.1007/s12154-016-0157-5.

Guo, C., Irudayaraj, J., 2011. Fluorescent Ag clusters via a protein-directed approach as a Hg (II) ion...Fluorescent Ag clusters via a protein-directed approach as a Hg (II) ion... Fluorescent Ag clusters via a protein-directed approach as a Hg (II) ion sensor 9–11. https://doi.org/10.1021/ac1032403.

Harika, V.K., Kumar, V.B., Gedanken, A., 2018. One-pot sonochemical synthesis of Hg–Ag alloy microspheres from liquid mercury. Ultrason. Sonochem. 40, 157–165. https://doi.org/10.1016/j.ultsonch.2017.07.008.

Harika, V.K., Sadhanala, H.K., Perelshtein, I., Gedanken, A., 2020. Sonication-assisted synthesis of bimetallic Hg/Pd alloy nanoparticles for catalytic reduction of nitrophenol and its derivatives. Ultrason. Sonochem. 60, 104804. https://doi.org/10.1016/j.ultsonch.2019.104804.

Harris, D.C., 2007. Quantitative Chemical Analysis, seventh ed. W. H. Freeman, New York.

Henglein, A., 1998. Colloidal silver nanoparticles: photochemical preparation and interaction with O_2, CCl_4, and some metal ions. Chem. Mater. 10, 444–450. https://doi.org/10.1021/cm970613j.

Henglein, A., Brancewicz, C., 1997. Absorption spectra and reactions of colloidal bimetallic nanoparticles containing mercury. Chem. Mater. 9, 2164–2167. https://doi.org/10.1021/cm970258x.

Inglezakis, V.J., Azat, S., Tauanov, Z., Mikhalovsky, S.V., 2021. Functionalization of biosourced silica and surface reactions with mercury in aqueous solutions. Chem. Eng. J. 423, 129745. https://doi.org/10.1016/j.cej.2021.129745.

Jarujamrus, P., Amatatongchai, M., Thima, A., Khongrangdee, T., Mongkontong, C., 2015. Selective colorimetric sensors based on the monitoring of an unmodified silver nanoparticles (AgNPs) reduction for a simple and rapid determination of mercury. Spectrochim. Acta Mol. Biomol. Spectrosc. 142, 86–93. https://doi.org/10.1016/j.saa.2015.01.084.

Jeevika, A., Shankaran, D.R., 2016. Functionalized silver nanoparticles probe for visual colorimetric sensing of mercury. Mater. Res. Bull. 83, 48–55. https://doi.org/10.1016/j.materresbull.2016.05.029.

Kang, H., Xiu, Z., Chen, J., Cao, W., Guo, Y., Li, T., Jin, Z., 2012. Reduction of nitrate by bimetallic Fe/Ni nanoparticles. Environ. Technol. 33, 2185–2192. https://doi.org/10.1080/09593330.2012.665486.

Karp, G., 2008. Cell and Molecular Biology, fifth ed. Wiley.

Katok, K.V., Whitby, R.L.D., Fayon, F., Bonnamy, S., Mikhalovsky, S.V., Cundy, A.B., 2013. Synthesis and application of hydride silica composites for rapid and facile removal of aqueous mercury. ChemPhysChem 14, 4126–4133. https://doi.org/10.1002/cphc.201300832.

Katok, K.V., Whitby, R.L.D., Fukuda, T., Maekawa, T., Bezverkhyy, I., Mikhalovsky, S.V., Cundy, A.B., 2012. Hyperstoichiometric interaction between silver and mercury at the nanoscale. Angewandte Chemie - International Edition 51, 2632–2635. https://doi.org/10.1002/anie.201106776.

Katsikas, L., Gutiérrez, M., Henglein, A., 1996. Bimetallic colloids: silver and mercury. J. Phys. Chem. 100, 11203–11206. https://doi.org/10.1021/jp960357i.

Kim, Y.H., Hahm, E., Pham, X.H., Kang, H., Jeong, D.H., Chang, H., Jun, B.H., 2023. Mercury ion-responsive coalescence of silver nanoparticles on a silica nanoparticle core for surface-enhanced Raman scattering sensing. ACS Appl. Nano Mater. 6, 23469–23476. https://doi.org/10.1021/acsanm.3c04843.

Kobayashi, G., Hinuma, Y., Matsuoka, S., Watanabe, A., Iqbal, M., Hirayama, M., Yonemura, M., Kamiyama, T., Tanaka, I., Kanno, R., 2016. Pure H- conduction in oxyhydrides. Science 351 (1979), 1314–1317. https://doi.org/10.1126/science.aac9185.

Lisha, K.P., Anshup, Pradeep, T., 2009. Towards a practical solution for removing inorganic mercury from drinking water using gold nanoparticles. Gold Bull. 42, 144–152. https://doi.org/10.1007/BF03214924.

Liu, Y., Huang, C.Z., 2013. Real-time dark-field scattering microscopic monitoring of the in situ growth of single ag@hg nanoalloys. ACS Nano 7, 11026–11034. https://doi.org/10.1021/nn404694e.

Lowe, B.M., Skylaris, C.K., Green, N.G., 2015. Acid-base dissociation mechanisms and energetics at the silica-water interface: an activationless process. J. Colloid Interface Sci. 451, 231–244. https://doi.org/10.1016/j.jcis.2015.01.094.

Mertens, S.F.L., Gara, M., Sologubenko, A.S., Mayer, J., Szidat, S., Krämer, K.W., Jacob, T., Schiffrin, D.J., Wandlowski, T., 2011. Au@Hg nanoalloy formation through direct amalgamation: structural, spectroscopic, and computational evidence for slow nanoscale diffusion. Adv. Funct. Mater. 21, 3259–3267. https://doi.org/10.1002/adfm.201100409.

Mustafa, S., Dilara, B., Naeem, A., Rehana, N., Nargis, K., 2003. Temperature and pH effect on the sorption of divalent metal ions by silica gel. Adsorpt. Sci. Technol. 21, 297–307. https://doi.org/10.1260/026361703322405033.

Ojea-Jiménez, I., López, X., Arbiol, J., Puntes, V., 2012. Citrate-coated gold nanoparticles as smart scavengers for mercury(II) removal from polluted waters. ACS Nano 6, 2253–2260. https://doi.org/10.1021/nn204313a.

Pang, J.T.T., Ritchie, I.M., 1982. The reactions between mercury ions and silver: dissolution and displacements. Electrochim. Acta 27, 683–689. https://doi.org/10.1016/0013-4686(82)85060-3.

Panichev, N., Kalumba, M.M., Mandiwana, K.L., 2014. Solid phase extraction of trace amount of mercury from natural waters on silver and gold nanoparticles. Anal. Chim. Acta 813, 56–62. https://doi.org/10.1016/j.aca.2014.01.011.

Pasakarnis, T.S., Boyanov, M.I., Kemner, K.M., Mishra, B., O'Loughlin, E.J., Parkin, G., Scherer, M.M., 2013. Influence of chloride and Fe(II) content on the reduction of Hg (II) by magnetite. Environ. Sci. Technol. 47, 6987–6994. https://doi.org/10.1021/es304761u.

Reed-Mundell, J.J., Nadkarni, D.V., Kunz, J.M., Fry, C.W., Fry, J.L., 1995. Formation of new materials with thin metal layers through "directed" reduction of ions at surface-immobilized silyl hydride functional groups. Silver on silica. Chem. Mater. 7, 1655–1660. https://doi.org/10.1021/cm00057a012.

Schopf, C., Martín, A., Iacopino, D., 2017. Plasmonic detection of mercury via amalgam formation on surface-immobilized single Au nanorods. Sci. Technol. Adv. Mater. 18, 60–67. https://doi.org/10.1080/14686996.2016.1258293.

Schopf, C., Martín, A., Schmidt, M., Iacopino, D., 2015. Investigation of Au-Hg amalgam formation on substrate-immobilized individual Au nanorods. J Mater Chem C Mater 3, 8865–8872. https://doi.org/10.1039/c5tc01800e.

Serruya, A., Mostany, J., Scharifker, B.R., 1999. Kinetics of mercury nucleation from Hg22+ and Hg2+ solutions on vitreous carbon electrodes. J. Electroanal. Chem. 464, 39–47. https://doi.org/10.1016/S0022-0728(98)00464-1.

Spanu, D., Bestetti, A., Hildebrand, H., Schmuki, P., Altomare, M., Recchia, S., 2019. Photocatalytic reduction and scavenging of Hg(ii) over templated-dewetted Au on TiO 2 nanotubes. Photochem. Photobiol. Sci. 18, 1046–1055. https://doi.org/10.1039/c8pp00424b.

Sumesh, E., Bootharaju, M.S., Anshup, Pradeep, T., 2011. A practical silver nanoparticle-based adsorbent for the removal of Hg2+ from water. J. Hazard Mater. 189, 450–457. https://doi.org/10.1016/j.jhazmat.2011.02.061.

Tauanov, Z., Lee, J., Inglezakis, V.J., 2020. Mercury reduction and chemisorption on the surface of synthetic zeolite silver nanocomposites: equilibrium studies and mechanisms. J. Mol. Liq. 305, 112825. https://doi.org/10.1016/j.molliq.2020.112825.

Tauanov, Z., Tsakiridis, P.E., Mikhalovsky, S.V., Inglezakis, V.J., 2018. Synthetic coal fly ash-derived zeolites doped with silver nanoparticles for mercury (II) removal from water. J Environ Manage 224, 164–171. https://doi.org/10.1016/j.jenvman.2018.07.049.

Tauanov, Z., Tsakiridis, P.E., Shah, D., Inglezakis, V.J., 2019. Synthetic sodalite doped with silver nanoparticles: characterization and mercury (II) removal from aqueous solutions. J Environ Sci Health A Tox Hazard Subst Environ Eng 54, 951–959. https://doi.org/10.1080/10934529.2019.1611129.

Tertykh, V.A., Ivashchenko, N.A., Yanishpolskii, V.V., Khainakov, S.A., 2013. Platinum nanoparticles on the surface of silica modified with silicon hydride groups. Materwiss Werksttech 44, 239–243. https://doi.org/10.1002/mawe.201300115.

Tiffreau, C., Lützenkirchen, J., Behra, P., 1995. Modeling the adsorption of mercury(II) on (Hydr)oxides. J. Colloid Interface Sci. https://doi.org/10.1006/jcis.1995.1228.

Tunsu, C., Wickman, B., 2018. Effective removal of mercury from aqueous streams via electrochemical alloy formation on platinum. Nat. Commun. 9, 4876. https://doi.org/10.1038/s41467-018-07300-z.

Wang, J.G., Fossey, J.S., Li, M., Xie, T., Long, Y.T., 2016. Real-time plasmonic monitoring of single gold amalgam nanoalloy electrochemical formation and stripping. ACS Appl. Mater. Interfaces 8, 8305–8314. https://doi.org/10.1021/acsami.6b01029.

Wang, L., Xu, H., Qiu, Y., Liu, X., Huang, W., Yan, N., Qu, Z., 2019. Utilization of Ag nanoparticles anchored in covalent organic frameworks for mercury removal from acidic waste water. J. Hazard Mater. 121824. https://doi.org/10.1016/j.jhazmat.2019.121824.

Wu, S.H., Lin, H.P., 2013. Synthesis of mesoporous silica nanoparticles. Chem. Soc. Rev. 42, 3862–3875. https://doi.org/10.1039/c3cs35405a.

Xu, D., Yu, S., Yin, Y., Wang, S., Lin, Q., Yuan, Z., 2018. Sensitive colorimetric Hg 2+ detection via amalgamation-mediated shape transition of gold nanostars. Front. Chem. 6, 1–9. https://doi.org/10.3389/fchem.2018.00566.

Yang, W., Chen, S., Ren, W., Zhao, Y., Chen, X., Jia, C., Liu, J., Zhao, C., 2019. Nanostructured amalgams with tuneable silver-mercury bonding sites for selective electroreduction of carbon dioxide into formate and carbon monoxide. J Mater Chem A Mater 7, 15907–15912. https://doi.org/10.1039/c9ta03611c.

Yordanova, T., Vasileva, P., Karadjova, I., 2022. Noble metal nanocomposites as tools for fast and reliable speciation analysis of mercury in water samples. Int. J. Environ. Anal. Chem. 102, 1152–1170. https://doi.org/10.1080/03067319.2020.1734193.

Yordanova, T., Vasileva, P., Karadjova, I., Nihtianova, D., 2014. Submicron silica spheres decorated with silver nanoparticles as a new effective sorbent for inorganic mercury in surface waters. Analyst 139, 1532–1540. https://doi.org/10.1039/c3an01279d.

Zangeneh Kamali, K., Pandikumar, A., Jayabal, S., Ramaraj, R., Lim, H.N., Ong, B.H., Bien, C.S.D., Kee, Y.Y., Huang, N.M., 2016. Amalgamation based optical and colorimetric sensing of mercury(II) ions with silver@graphene oxide nanocomposite materials. Microchim. Acta 183, 369–377. https://doi.org/10.1007/s00604-015-1658-6.

Zhu, I., Getting, T., 2012. A review of nitrate reduction using inorganic materials. Environmental Technology Reviews 1, 46–58. https://doi.org/10.1080/09593330.2012.706646.

Zienkiewicz-Strzałka, M., Deryło-Marczewska, A., Kozakevych, R.B., 2018. Silica nanocomposites based on silver nanoparticles-functionalization and pH effect. Appl. Nanosci. 8, 1649–1668. https://doi.org/10.1007/s13204-018-0837-2.